High harmonic generation in systems with bounded chaos

W. Chism, T. Timberlake, and L. E. Reichl
Center for Studies in Statistical Mechanics and Complex Systems, The University of Texas at Austin, Austin, Texas 78712
(Received 22 December 1997)

In this paper we study the radiation spectrum generated by the quantum dynamics of a double resonance model and a driven square well system. We use Floquet theory to analyze the radiation generated by these systems. We present the results of numerical simulations that indicate a connection between high harmonic generation and underlying classical chaos in these models. Our results provide a means of predicting the radiative characteristics of multilevel quantum systems subject to a strong periodic driving force. [S1063-651X(98)02308-3]

PACS number(s): 05.45.+b, 42.50.Hz, 42.65.Ky

I. INTRODUCTION

High harmonic generation (HHG) by atoms subject to intense laser pulses is a major topic in nonlinear atomic physics. The characteristic radiation spectrum of strongly driven atomic systems consists of a rapid decrease in radiated intensity over the first few laser harmonics followed by a plateau of approximately equal intensity peaks out to an abrupt cutoff. For atoms subject to low frequency driving fields $\omega_0 \leqslant I_p$, where ω_0 is the driving frequency and I_p is the ionization potential, electron ionization and subsequent recombination account for the cutoff location. If the driving frequency is lower than the tunneling frequency, given by $F/\sqrt{2I_p}$, where F is the field strength, the electron will tunnel through the quasistatic barrier [1]. It may gain energy from the laser field and recombine, emitting high frequency radiation. The energy gained by the electron is determined by the phase of the driving field at the instant the electron tunnels. The maximum energy that can be gained by an electron that returns to the core is $3.17U_p$, where U_p is the cycle averaged electron energy in the laser field: $F^2/4\omega_0^2$ [2–4]. Thus a two-step ionization and recombination process accounts for the experimentally observed cutoff law.

However, high harmonic generation has proved general to all known strongly driven quantum systems, including those that allow no ionization. Several examples are the driven two-level model [5], the driven triangular well [6], and the driven anharmonic oscillator [7]. The location of the cutoff in these systems is clearly not due to ionization and recombination. Recently, Gauthey *et al.* [8] have shown the cutoff in the two-level model to be given by $\omega_{max} \simeq \omega_{ab}/2 + 2\Omega$, where Ω is the Rabi frequency $2dF/\hbar$ and $\hbar\omega_{ab} \equiv E_a - E_b$. As usual, d is the off-diagonal dipole matrix element and E_a and E_b are the energy eigenvalues. The 2Ω term can be viewed as arising from the dynamical Stark shift of either state. Thus this term represents the kinetic energy attainable from the driving field. This sets the gain curve (the frequency range over which the system may respond) analogous to the $3.17U_p$ term in the tunneling regime, although the cutoff dependence on field strength is quite different.

In this paper, we consider mechanisms for HHG in multilevel quantum systems driven by time periodic semiclassical force fields. The classical counterpart of such systems can exhibit a transition to chaos [9]. It is well known that chaos in a classical system will allow a particle to diffuse throughout the chaotic region, sampling a range of energies. By transforming the classical Hamiltonian of a particle subject to a strong driving force to action-angle variables, the Hamiltonian, in general, will take the form

$$H = E_0(J) + F \sum_{m=-\infty}^{\infty} x_m(J)\cos(m\theta - \omega t), \qquad (1.1)$$

where $|\theta| \leqslant 2\pi$ and $x_m(J) = \pi^{-1}\int_0^{2\pi} x(J,\theta)\cos(m\theta)d\theta$. Thus the driving field induces an infinite series of nonlinear pendulumlike resonances with location given by $\partial E_0/\partial J \approx \omega/m$. An isolated resonance will have classical width $\Delta J_m \propto F^{1/2}$. For sufficiently strong fields these resonances will overlap and lead to chaos in the phase space. The presence of chaos in a classical model driven by a strong periodic force indicates the corresponding quantum system might sample a wider range of energies, gain kinetic energy from the driving field, and radiate harmonics of the driving frequency. Averbukh and Moiseyev [10] found that the harmonic cutoff in the double resonance model is given by the extent in energy of the underlying classical chaos.

In this paper we use Floquet analysis [9,11,12] to examine the relationship between chaos in classical systems and HHG in their quantum counterpart. We will look first at the classical and quantum versions of the paradigm system for the generation of chaos: the double resonance model. This model is important for theoretical studies of renormalization in classical and quantum dynamics [9,13]. Then we carry out a study of the classical and quantum dynamics of the driven square well, which may be more easily realized in laboratory experiments [14]. Both these systems contain regions of confined chaos.

II. DOUBLE RESONANCE MODEL

In this section, we examine the classical and quantum dynamics of the simplest Hamiltonian system that exhibits a transition to chaos, the double resonance model [9,13,15,16]. We use Floquet theory to make the connection between HHG and classical structures, similar to the analysis of Averbukh and Moiseyev [10]. However, we consider the radiation

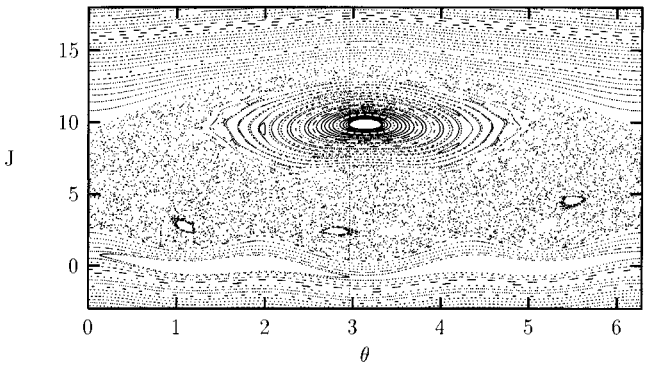

FIG. 1. Strobe plot showing the classical phase space of the double resonance model with parameters $V_1=4.5$, $V_2=V_1/4$, $M_1=1$, $M_2=3$, and $\omega_0=9.7$. The M_1 resonance, located at $J_1\approx 9.7$, has overlapped with the M_2 resonance. The M_2 resonance, initially located at $J_2\approx\omega_0/M_2=3.23$, has been almost completely destroyed.

produced by superpositions of Floquet states excited during the turn-on of the periodic interaction and the effect of chaos on those superpositions.

A. Classical model

The double resonance Hamiltonian consists of a rotor driven by a pair of traveling sinusoidal potential waves

$$H=\frac{J^2}{2I}+V_1\cos(M_1\theta-\omega_0 t)+V_2\cos(M_2\theta-\omega_0 t), \tag{2.1}$$

where J is the angular momentum of the rotor, θ ($|\theta|\leqslant 2\pi$) is its angle, I is the rotor's moment of inertia, the V_i are the wave amplitudes, and the wave speeds are $\dot{\theta}=\omega_0/M_i$. We rescale this Hamiltonian to dimensionless units by taking $J\rightarrow J\hbar$, $t\rightarrow t\hbar/I$, $V_i\rightarrow V_i\hbar^2/I$, $\omega_0\rightarrow\omega_0 I/\hbar$, and $H\rightarrow H\hbar^2/I$. This yields

$$H=\frac{J^2}{2}+V_1\cos(M_1\theta-\omega_0 t)+V_2\cos(M_2\theta-\omega_0 t). \tag{2.2}$$

This system models the dynamics in the vicinity of a pair of nonlinear resonances, as in the action-angle Hamiltonian for an atom subject to a strong periodic driving field. It has two primary resonances that may interact, producing higher-order nonlinear resonances and chaos in the phase space. The primary resonances lie at $J_i=\omega_0/M_i$ with $i=1,2$.

Figure 1 shows the phase space for this system using $M_1=1$, $M_2=3$, $\omega_0=9.7$, $V_1=4.5$, and $V_2=V_1/4$. The resonances are located at $J_1\approx 9.7$ and $J_2\approx 3.23$. From the strobe plot we see that there are three distinct phase space structures for this field strength. There are regions above and below the resonances corresponding to integrable or ''regular'' motion. The primary nonlinear resonances have begun to overlap and create a network of higher-order resonances. This produces a regular region within the large primary resonance, surrounded by a chaotic strip in the phase space. A particle that starts out in the chaotic region may sample energies throughout this region, while a particle trapped in the remaining larger primary has a maximal kinetic energy range determined by the width of the resonance. The kinetic energy accessible to a classical particle in the chaotic region is $J_{max}^2/2-J_{min}^2/2$, where J_{max} and J_{min} are the upper and lower bounds in action of the chaotic strip. Dividing this by the driving frequency gives the maximum expected harmonic frequency component of the particle motion. From the strobe plot, we see this is near the tenth harmonic. For the particle trapped inside the M_1 resonance, the classically predicted cutoff is near the fifth harmonic.

B. Quantum model

We now study the radiation generated by the quantum version of the paradigm system. Taking $J\rightarrow\hat{J}=-i(\partial/\partial\theta)$, the Schrödinger equation becomes

$$i\frac{\partial\Psi(\theta,t)}{\partial t}=-\frac{1}{2}\frac{\partial^2\Psi(\theta,t)}{\partial\theta^2}+\xi(t)[V_1\cos(M_1\theta-\omega_0 t)+V_2\cos(M_2\theta-\omega_0 t)]\Psi(\theta,t), \tag{2.3}$$

where $\xi(t)$ is the turn-on function.

For all of the calculations in this paper we will use a turn-on function given by

$$\xi(t)=\begin{cases}\sin^2\left(\dfrac{\omega_0 t}{4\nu}\right), & t<\dfrac{2\pi\nu}{\omega_0}\\[2ex] 1, & t>\dfrac{2\pi\nu}{\omega_0},\end{cases} \tag{2.4}$$

where ν is the number of cycles in the turn-on. After the turn-on, the Hamiltonian is invariant under the discrete time translation symmetry $t\rightarrow t\pm 2\pi/\omega_0$. This allows us to analyze the system in terms of eigenstates of the unitary one-period time evolution operator (Floquet states) [11,12]. In order to obtain the Floquet states, we represent the full time-periodic Hamiltonian in the rotor basis. Then we integrate the Schrödinger equation N times (N is the number of basis states) from $t=0$ to $t=T$ with initial conditions $|\Psi(t=0)\rangle=|n\rangle$ ($1\leqslant n\leqslant N$), where $|n\rangle$ is the nth unperturbed energy eigenstate. Each integration gives one column of the matrix representation of the unitary time evolution operator. Eigenvectors of this operator are the Floquet states $|\Omega_\alpha\rangle$, which satisfy

$$\hat{U}(T)\,|\Omega_\alpha\rangle=e^{i\Omega_\alpha T}\,|\Omega_\alpha\rangle, \tag{2.5}$$

where Ω_α is the Floquet eigenvalue (or quasienergy). Solving the eigenvalue problem, we obtain representations of N Floquet states [9]. These are steady states of the atom plus driving field, in analogy with steady states of the time-independent problem. After the turn-on, we project the wave function onto the Floquet basis to determine which states are populated. We then use the Husimi distribution (see Appendix A) on quantum-mechanical phase space to relate these states to classical structures.

Expanding the Schrödinger equation in free rotor eigenstates $\langle\theta|n\rangle=(1/\sqrt{2\pi})e^{in\theta}$, we obtain an ordinary differential equation for the time-dependent coefficients:

$$i\dot{\psi}_n=\frac{n^2}{2}\psi_n+\frac{V_1}{2}(e^{-i\omega_0 t}\psi_{n-M_1}+e^{i\omega_0 t}\psi_{n+M_1})$$

$$+\frac{V_2}{2}(e^{-i\omega_0 t}\psi_{n-M_2}+e^{i\omega_0 t}\psi_{n+M_2}). \tag{2.6}$$

The acceleration time series is given by

$$\langle\Psi(t)|\ddot{\hat{\theta}}|\Psi(t)\rangle=\sum_{kl}\Psi_k^*(t)\Psi_l(t)\ddot{\theta}_{kl}, \tag{2.7}$$

where

$$\ddot{\theta}_{kl}=\sum_{ij}[2\langle k|\hat{H}|i\rangle\langle i|\hat{\theta}|j\rangle\langle j|\hat{H}|l\rangle-\langle k|\hat{H}|i\rangle\langle i|\hat{H}|j\rangle\langle j|\hat{\theta}|l\rangle$$

$$-\langle k|\hat{\theta}|i\rangle\langle i|\hat{H}|j\rangle\langle j|\hat{H}|l\rangle] \tag{2.8}$$

and

$$\theta_{kl}\equiv\langle k|\theta|l\rangle=\begin{cases}\pi, & k=l\\ \dfrac{i}{k-l}, & k\neq l.\end{cases} \tag{2.9}$$

We show the radiation spectrum for this system obtained from integrating the Schrödinger equation with parameter values identical to the classical case. Figure 2 shows the log power spectrum for $\omega_0=9.7$ and various initial atomic states. These show the radiative characteristics for the atomic system prepared in each of the three distinct classical regions. In each case, we turn on the interaction with the $\sin^2$ ramping over 16 cycles, followed by constant amplitude for 32 cycles. The acceleration time series is calculated from the constant amplitude integration. The power spectrum is estimated by taking the modulus squared of the Fourier transform $\chi(\omega)$ of the acceleration time series. Note that we do not expect even harmonics to be forbidden, as in realistic atomic systems, since the Hamiltonian is not invariant under $\theta\rightarrow-\theta$.

Figure 2(a) shows the spectrum typical of a quantum system excited into a state or set of states that has regular underlying classical dynamics. There is no significant harmonic generation. The individual Floquet states, which are the stationary states of the atom plus laser system, have support localized to a narrow band of atomic states. Thus a singly excited Floquet state will possess a narrow gain curve (see Appendix B).

Figure 2(b) shows a typical spectrum for a quantum system with underlying classical chaos: Radiation is produced with the gain curve approximately given by the width in kinetic energy of the chaotic strip. The spectrum shows a cutoff near the tenth harmonic, in agreement with the classical prediction. Projection of the initial wave function (after turn-on) onto the Floquet basis shows several states with reasonable population. This is not unexpected since the states do not evolve perfectly adiabatically for the finite turn-on. The quasienergies of the initially populated states determine the detailed structure of the radiation spectrum without affecting the location of the cutoff. This is because Floquet states may become ''broadened'' across the classically irregular region, gaining support on atomic states throughout the chaotic region [17,18]. Thus a single Floquet state, with support across the chaotic region, generates only pure harmonics of the driving field (see Appendix B), with the cutoff given by the width in energy of the chaotic strip. The presence of shifted harmonics is an indication that multiple broadened Floquet states are contributing [19,20]. Figures 3(a)–3(c) show the Floquet states involved in production of the radiation seen in Fig. 2(b).

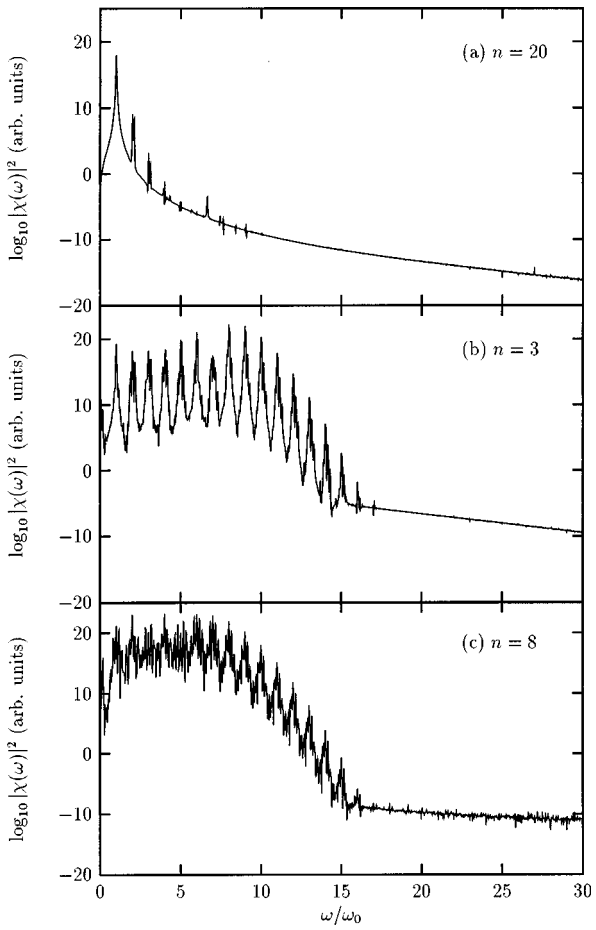

FIG. 2. Radiation spectrum for states initially localized to the three distinct classical regions of the double resonance model. For each case, the rotor is placed in an initial state n and the interaction is ramped on with a 16 cycle turn-on. The typical spectrum corresponding to ''regular'' regions is shown in (a) where $n=20$. The typical spectrum for ''chaotic'' initial conditions is shown in (b), where $n=3$. The radiation produced by a superposition of ''resonance'' states is shown in (c), where $n=8$.

Figure 2(c) shows the radiation spectrum of a typical atomic system trapped in a single nonlinear resonance. It has many shifted harmonics (hyper-Raman lines) and a cutoff given by the width in energy of the nonlinear resonance. For the M_1 primary resonance, the classically predicted cutoff is at about the fifth harmonic, which agrees well with the cutoff in Fig. 2(c). The many shifted peaks indicate the excitation of many Floquet states associated with the resonance. Figures 3(d)–3(f) show the Husimi distributions for several of these ''resonance'' states.

Our results describe the radiative characteristics of Floquet states associated with these three distinct regions in classical phase space. The results we have seen for the double resonance model should be applicable to all strongly driven multilevel systems, where regular regions, nonlinear

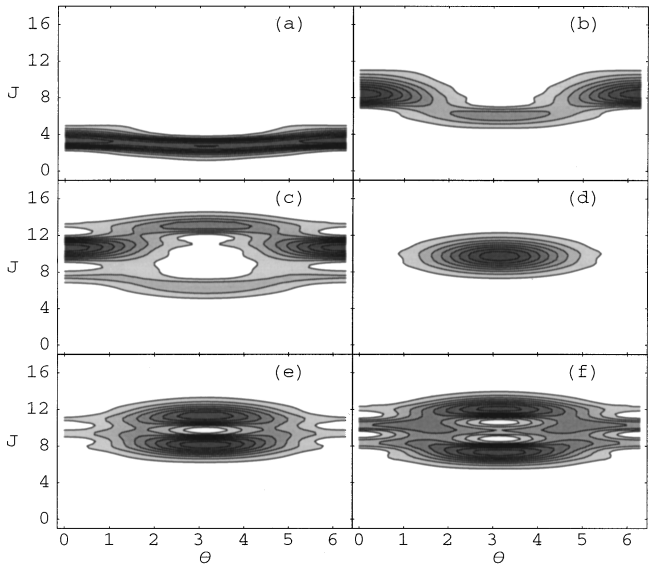

FIG. 3. Husimi distributions of Floquet states responsible for radiation shown in Figs. 2(b)–2(c). In (a)–(c), we show the set of Floquet states responsible for the harmonic generation shown in Fig. 2(b). In (d)–(f) we show the ''nonlinear resonance'' Floquet states responsible for radiation shown in Fig. 2(c).

resonances, and chaos coexist in phase space.

III. DRIVEN PARTICLE IN A SQUARE WELL POTENTIAL

The rest of the paper will be devoted to studying a particle confined to an infinitely deep square well and driven by a time-periodic field. The infinite square well is representative of a class of systems whose potential is of the form $V(x)=x^{2n}$ for $n\geqslant 2$ (it is the $n\to\infty$ limit of this form). Any classical system of this type will develop nonlinear resonances at low energies when it is driven by a periodic force. These resonances can overlap and create a region of chaos that is bounded from above [21,22]. The quantum versions of these systems also have features corresponding to classical nonlinear resonances [23,24]. These structures have important effects, similar to those that were seen in the double resonance model, on the radiation spectra of these systems.

A. Classical system

The Hamiltonian for the driven square well is

$$\tilde{H}=\frac{\tilde{p}^2}{2m}+\tilde{\epsilon}\tilde{x}\cos\tilde{\omega}_0\tilde{t},\quad |\tilde{x}|\leqslant a, \tag{3.1}$$

where m is the mass, $\tilde{p}$ is the momentum, and $\tilde{x}$ is the position of the particle. The width of the square well is $2a$. The driving field has amplitude $\tilde{\epsilon}$ and frequency $\tilde{\omega}_0$, with $\tilde{t}$ as the time coordinate. This Hamiltonian can be made dimensionless using the scaling transformation introduced in [21], where $\tilde{H}=Hc$, $\tilde{x}=xa$, $\tilde{p}=p\sqrt{2mc}$, $\tilde{\epsilon}=\epsilon(c/a)$, $\tilde{t}=ta\sqrt{2m/c}$, and $\tilde{\omega}_0=\omega_0(1/a)\sqrt{c/2m}$. This transformation introduces an arbitrary unit of energy c. The scaled Hamiltonian (in units of c) is

$$H=p^2+\epsilon x\cos\omega_0 t,\quad |x|\leqslant 1, \tag{3.2}$$

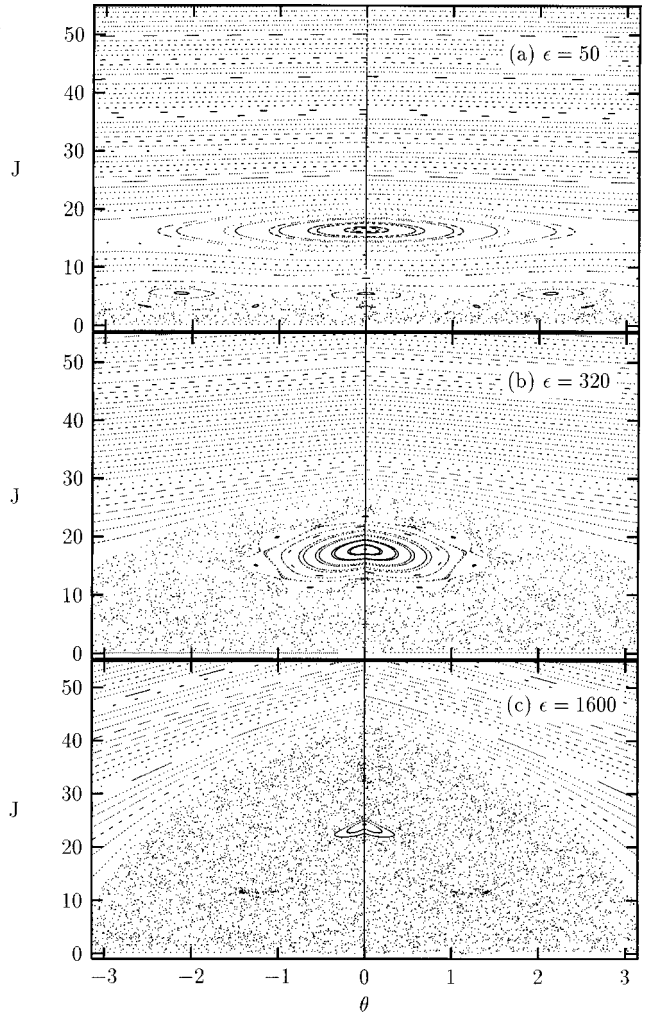

FIG. 4. Strobe plots of the classical phase space for the driven square well. Primary resonances overlap and form a bounded region of chaos as ϵ is increased. The line at $\theta=0$ indicates the presence of a hard wall ($\theta=0\leftrightarrow x=-1$).

where all quantities are now dimensionless.

Note that ϵ and ω_0 are not independent parameters since the transformation $(\omega_0,\epsilon)\to(\omega_0\sqrt{c},\epsilon c)$ produces the same dynamics (with a rescaling of the energy unit c). Because of this scaling law we can choose an arbitrary ω_0, study the dynamics as a function of ϵ, and effectively analyze the dynamics for any set of (ω_0,ϵ). In this paper we choose $\omega_0=80$. Figure 4 shows strobe plots of this system (in action-angle variables) for $\epsilon=50$, 320, and 1600.

We can rewrite this Hamiltonian using action-angle variables. We find

$$H=\frac{\pi^2J^2}{4}-\frac{8\epsilon}{\pi^2}\sum_{\substack{n=-\infty\\ n\ \text{odd}}}^{\infty}\frac{1}{n^2}\cos(n\theta-\omega_0 t). \tag{3.3}$$

The action and angle variables are defined by $J=2|p|/\pi$ and $\theta=\pm\pi(x+1)/2$. This form of the Hamiltonian indicates that primary resonances for the driven system occur at values of the action variable given by $J_c^m=2\omega_0/m\pi^2$. The $m=1$ resonance is apparent in all of the strobe plots in Fig. 4. The $m=3$ resonance is visible only in the $\epsilon=50$ plot. For ϵ

=320 and 1600 all of the primary resonances have overlapped and all but the $m=1$ resonance have been destroyed. Note that the $m=1$ resonance cannot overlap with any higher energy primary resonances because there are no primary resonances with a higher energy. Thus the region above the $m=1$ resonance will remain regular for all field strengths. This leads to ''bounded chaos'' in the system. We will show that this structure has a profound effect on the dynamics of the corresponding quantum system.

B. Quantum system

The Schrödinger equation for a driven particle in an infinite square well is given by

$$i\hbar\frac{\partial}{\partial t}|\psi(t)\rangle=[H_0+\epsilon\xi(t)x\cos(\Omega t)]|\psi(t)\rangle, \quad (3.4)$$

where H_0 is the Hamiltonian for the undriven system (i.e., $H_0=p^2$, $|x|\leqslant 1$) and $\xi(t)$ is the turn-on function [see Eq. (2.4)]. For all square well calculations we use $\hbar=1$.

Again we use the eigenstates of H_0 to analyze the Schrödinger equation for this system. The boundary conditions for the eigenstates of H_0 are $\psi(-1,t)=\psi(1,t)=0$, where $\psi(x,t)=\langle x|\psi(t)\rangle$. The energy eigenvalues of H_0 are

$$E_n=\frac{\pi^2\hbar^2n^2}{4}, \quad n=1,2,\ldots, \quad (3.5)$$

and the corresponding wave functions are given by

$$\psi_n(x)=\langle x|E_n\rangle=\sin\left(\frac{\pi n(x-1)}{2}\right), \quad (3.6)$$

where $|E_n\rangle$ represents the eigenstate whose eigenvalue is E_n. The dipole matrix elements for these eigenstates are

$$x_{nm}=\begin{cases}0, & m+n(\mathrm{mod}\,2)=0\\ \dfrac{16mn}{\pi^2(m^2-n^2)^2}, & m+n(\mathrm{mod}\,2)=1,\end{cases} \quad (3.7)$$

where (mod 2) stands for ''modulo 2.'' This form is very convenient for numerical calculations.

Writing the wave function in the energy basis [$|\psi(t)\rangle=\Sigma_i c_i(t)|E_i\rangle$], one can convert the Schrödinger equation into a system of ordinary differential equations for the c_i's:

$$\frac{dc_i(t)}{dt}=-\frac{iE_i}{\hbar}c_i(t)+\frac{i}{\hbar}\epsilon\xi(t)\cos(\omega_0t)\sum_j x_{ij}c_j(t). \quad (3.8)$$

This system can be numerically solved for any initial condition. The radiation spectrum is simply the Fourier transform of the acceleration, and the acceleration time series is given by

$$\langle\psi(t)|\ddot{x}|\psi(t)\rangle=\sum_{i,j} c_j^*(t)\ddot{x}_{ji}c_i(t), \quad (3.9)$$

where

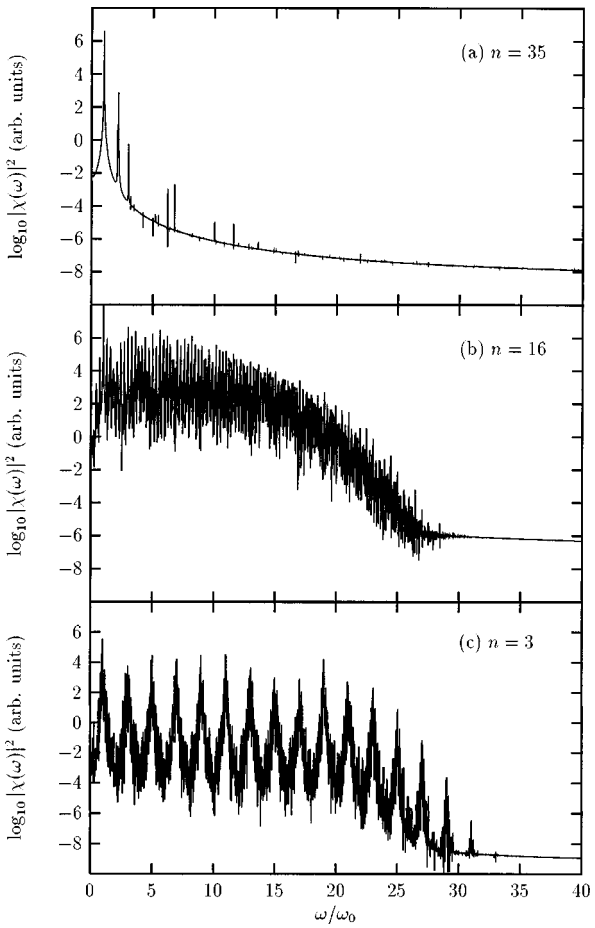

FIG. 5. Spectra for the driven square well at $\epsilon=320$. These three spectra are typical for initial conditions starting in the three regions of classical phase space: (a) regular, (b) resonance, and (c) chaotic. The cutoffs for (b) and (c) are determined by the range of energies a classical particle in each region can sample.

$$\ddot{x}_{ji}=-\frac{1}{\hbar^2}(E_j-E_i)^2x_{ji}+\frac{1}{\hbar^2}\epsilon\xi(t)\cos(\omega_0t)\sum_k (2E_k-E_j-E_i)x_{jk}x_{ki} \quad (3.10)$$

is the ''acceleration matrix element.''

We use a basis of the first 80 eigenstates of H_0, which extends well into the regular region for all of the field strengths we will consider. All spectra were calculated using 128 cycles of the field after the end of the initial turn-on period. Examples of spectra are shown in Fig. 5. Note that since parity is a good quantum number for this system there is no radiation at even harmonics of the driving field.

IV. HARMONIC GENERATION IN THE SQUARE WELL

We study harmonic generation in the quantum system for two field strengths. At each field strength we calculate the radiation spectrum, and Floquet composition at the end of the turn-on, for several initial states. In each case the spectrum is essentially determined by which Floquet states are

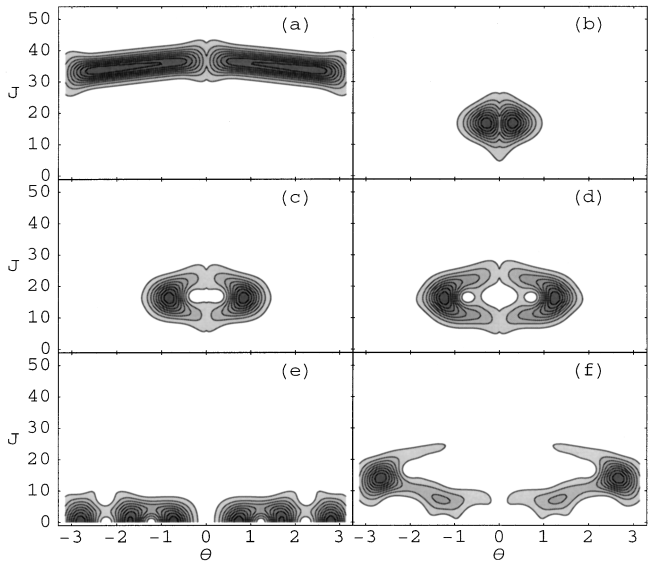

FIG. 6. Husimi plots of Floquet states for the driven square well at $\epsilon = 320$. Each state can be associated with a particular region of the classical phase space: (a) regular, (b)–(d) resonance, and (e) and (f) chaotic.

excited. For a general discussion on the radiation spectrum of a superposition of Floquet states see Appendix B.

A. Strong field

The classical phase space for field strength $\epsilon = 320$ is chaotic for actions less than about 25. However, in the middle of this chaotic sea there is a prominent resonance from 12 to 22 in action and about -1 to 1 in angle. Above $J = 25$ the phase space is regular.

We compute the radiation spectrum of the quantum system for three different initial conditions $n = 3$, $n = 16$, and $n = 35$. This allows us to study the quantum behavior for states that sit in the chaotic, resonance, and regular regions of the classical phase space. For this field strength we use a 12-cycle turn-on. The radiation spectrum for each initial condition is shown in Fig. 5.

For initial state $n = 35$ we see that there is no high harmonic generation. The radiation spectrum is typical of what we might find using perturbation theory at weak field strengths. There is no significant harmonic radiation. After computing the Floquet eigenstates for this field strength we find that only one Floquet state was excited for this initial condition. The Husimi distribution of that Floquet state is shown in Fig. 6(a). (Note that this and all Husimi distributions for this system should go to zero at $\theta = 0$ since this corresponds to $x = -1$. Because of the smoothing involved in creating the Husimi distribution there appears to be nonzero probability at $\theta = 0$ even though the *wave function* goes to zero there.) It is clear that the Husimi distribution closely follows the invariant tori that appear in the regular part of the classical phase space. We will call such a state a ''regular'' Floquet state. These states are typically excited for initial conditions that begin in the regular part of the classical phase space. Since these states produce no HHG, this region will be of little interest to us here.

For initial state $n = 16$ the radiation spectrum [Fig. 5(b)] is quite different. There does appear to be a plateau in the spectrum running out to about the 11th harmonic. However, the harmonic peaks do not show up clearly. There are a number of additional peaks (shifted harmonics) that make the spectrum very messy. The Floquet analysis reveals that about 13 Floquet states are excited above the level of 0.1%. This leads to shifted harmonics because the system can radiate at frequencies $n\omega_0 + (\Omega_\alpha - \Omega_\beta)$, where Ω_α and Ω_β are quasienergies associated with the excited Floquet states (Appendix B). If n Floquet states are excited there will be $(n-1)!$ possible values of $(\Omega_\alpha - \Omega_\beta)$. For 13 states this means nearly 10^9 possible shifted peaks for each harmonic. It should be noted, however, that 80% of the probability lies in three Floquet states. The Husimi distributions for these Floquet states are shown in Figs. 6(b)–6(d). These three states are all localized within the primary resonance.

Now for initial state $n = 3$ we see from Fig. 5(c) that there is strong harmonic generation. The cutoff in the spectrum appears to be at about the 19th harmonic. There are a few shifted peaks, but not so many as to obscure the harmonic peaks. The Floquet analysis reveals that there are two Floquet states that are significantly excited. We see that the Husimi distributions of these Floquet states, shown in Figs. 6(e) and 6(f), are concentrated in the chaotic region of the classical phase space. One of these is localized near $J = 0$ (the bottom of the well), while the other is localized near the unstable fixed point at $J \approx 15$. This combination gives the quantum system access to energies spanning the chaotic region.

For the combination of Floquet states arising from $n = 3$, one would expect transitions to occur whose energy difference is equal to the energy range of the chaotic region $[\Delta E = \pi^2(25^2 - 0^2)/4 = 1542]$ or less (see Appendix B). So the cutoff in the harmonic generation should occur at $\Delta E/\omega_0 = 1542/80 \approx 19$, which is exactly what we see in Fig. 5(c). For the resonance Floquet states arising from $n = 16$ one would expect the cutoff to be given by the energy range of the resonance divided by ω_0. We find $\Delta E_{res} = \pi^2(22^2 - 12^2)/4 = 839$ and $\Delta E_{res}/\Omega = 839/80 \approx 10.5$ which again fits the spectrum in Fig. 5(b).

B. Very strong field

At a field strength of $\epsilon = 1600$ the classical phase space is chaotic below $J = 40$, as seen in Fig. 4(c). There is a small resonance still present near $J = 22$, as well as some tiny secondary resonances, but all of these structures are small compared to $\hbar$ in the quantum system. We cannot expect these structures to have an impact on the quantum dynamics of the system. Above $J = 40$ the phase space is regular.

We study this field strength using initial conditions $n = 3$ and $n = 22$. We omit the results for $n > 40$ because they are identical to the regular results for $\epsilon = 320$ [see Figs. 5(a) and 6(a)]. The turn-on for this field strength is 60 cycles, which gives the same adiabaticity as the 12-cycle turn-on for $\epsilon = 320$.

Starting off in $n = 3$, we find the spectrum shown in Fig. 7(a). At low frequencies the radiation spectrum resembles ''white noise.'' This is because of the large number of shifted peaks that wash out the harmonics. The system

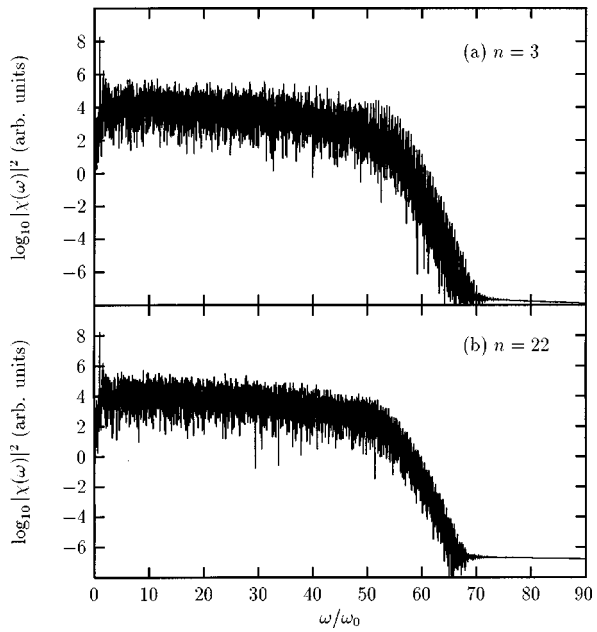

FIG. 7. Spectra for the driven square well at $\epsilon=1600$. Although (b) starts off in the resonance region, the resonance at this field strength is too small to influence the quantum dynamics. The cutoffs for both spectra are given by the energy range of the chaotic region.

passes through many avoided crossings (see Sec. V) during the turn-on, resulting in the excitation of many Floquet states. There appears to be a cutoff at about the 50th harmonic. We show the Husimi distributions of two of these Floquet states in Figs. 8(a) and 8(b). While the state shown in Fig. 8(a) appears to be concentrated near the location of the small resonance (although certainly not inside it), the state in Fig. 8(b) is spread throughout the chaotic region. This is somewhat different from the localized ''chaotic'' Floquet states at $\epsilon=320$. However, at this higher field strength it is typical for the chaotic Floquet states to fill the chaotic region. This delocalization occurs for Floquet states that have passed through many avoided crossings (see Sec. V). Again we see that the size of the chaotic region determines the cutoff as $\Delta E=\pi^2(40^2-0)/4=3948$ and $\Delta E/\omega_0=3948/80\approx 49$, which agree well with what we see in the spectrum.

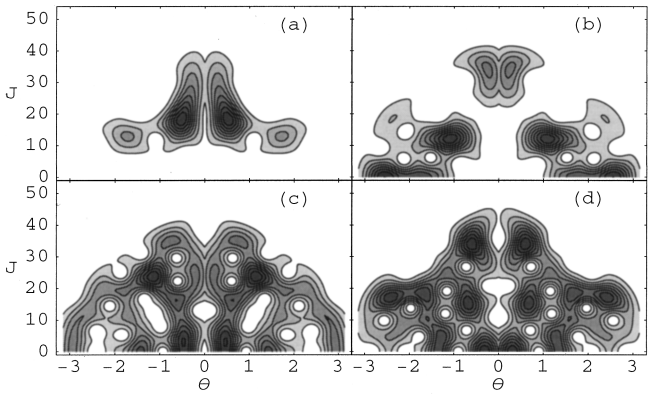

FIG. 8. Husimi plots for driven square well Floquet states at $\epsilon=1600$. At this high field strength the Floquet states broaden to fill the region of chaos.

At $n=22$ we are close to the energy of the small resonance. However, we see that the spectrum for this initial condition [Fig. 7(b)] looks very similar to the one for $n=3$. Again we find that there are many Floquet states populated. Husimi plots for two of these are shown in Figs. 8(c) and 8(d). It is clear that these states are *not* concentrated inside the small resonance. This is because the resonance is small compared to the size of $\hbar$ in our calculations. The quantum system effectively ignores the presence of the resonance. Instead, the system populates delocalized chaotic Floquet states, as for $n=3$. Again, the cutoff matches the energy range of the chaotic region.

C. General properties

From the above analysis we derive some basic properties of the radiation spectrum for this system. First, states that start out in a regular region of the classical phase space will remain localized in this region. They will typically only excite a single Floquet state whose Husimi distribution is concentrated around a classical invariant torus. Such a state will produce no HHG.

A state initially inside a large (relative to $\hbar$) resonance will typically excite numerous Floquet states. This large number of Floquet states leads to a noisy spectrum with many shifted peaks. However, most of the probability will be in Floquet states that are localized in or near the resonance region. This leads to a cutoff in the spectrum that is determined by the width (in energy) of the resonance.

An initial condition in the chaotic region will excite chaotic Floquet states. At lower field strengths these chaotic states will be localized near a particular unstable periodic orbit of the classical system. Only a few of these localized states will be excited, which leads to a clean harmonic spectrum. At very high field strengths the chaotic Floquet states will have Husimi distributions that fill the chaotic region. These delocalized states have become associated with a large set of periodic orbits of the classical system. This occurs when the system has passed through many avoided crossings during the turn-on. These avoided crossings lead to the excitation of a large number of Floquet states and an incoherent radiation spectrum. In either case the cutoff is given by the energy range of the chaos, which can be quite large.

In all of these cases the cutoff in the HHG is determined by the range of energies that the classical particle can sample during its trajectory. This result is in agreement with [10]. It is also similar to other cutoff laws (like those invoking the ponderomotive potential or the ac Stark shift) because the cutoff is just given by the maximum energy that the classical particle can gain from the field. For a state that is initially in a chaotic region we can predict the cutoff by examining a strobe plot of the classical dynamics. Table I shows the cutoffs seen in the spectra and the energy range of the chaos seen in the strobe plots. The observed cutoffs follow the strobe plot predictions very closely.

Note that the table includes data from field strengths that are not discussed elsewhere in this paper. The uncertainties in the cutoff values read from the spectra are worse for high field strengths because these spectra tend to be noisy and difficult to read.

TABLE I. Observed harmonic cutoffs and predictions based on classical strobe plots for several field strengths ϵ. Uncertainties in the observed cutoffs are large for very strong fields because these spectra have many shifted peaks, making them difficult to read.

ϵ	Observed	Strobe
50	9 ± 2	≈11
150	15 ± 2	≈15
320	19 ± 2	≈19
960	35 ± 2	≈37
1600	49 ± 4	≈49
2560	73 ± 4	≈74

V. AVOIDED CROSSINGS

It seems apparent from the above analysis that if one wishes to get HHG, one must excite chaotic Floquet states. To get sharp peaks at the harmonics (i.e., few shifted harmonics), one should excite as few Floquet states as possible [19,20]. Ideally one would like to excite a single delocalized Floquet state, but it is nearly impossible to excite only one such state. Another alternative is to excite a superposition of two states that sit at high and low energies, respectively. Avoided crossings in the Floquet spectrum provide the opportunity for transitions between Floquet states [25] and hence a method for engineering a particular combination of Floquet states.

In Fig. 9 we plot the quasienergies of our system for field strengths of 0–400. Up to field strengths of about $\epsilon=200$ there are few avoided crossings (where two curves approach, but do not cross each other) to be seen. However, after this point the avoided crossings arise quickly. At even higher field strengths almost every curve undergoes a rapid succession of many avoided crossings. The proliferation of avoided crossings is associated with the spread of chaos in the classical system. One of the first avoided crossings occurs at a field strength of $\epsilon\approx100$. This matches the critical field strength for overlap of the two highest energy primary resonances in this system [21,22]. This avoided crossing involves states connected to $n=6$ and $n=10$ (labeled Ω_6 and Ω_{10} in Fig. 9). We note that these pairs are symmetric about $n=8$ because $J=8$ is precisely where the classical resonances overlap at the critical field strength. This indicates a strong connection between avoided crossings in the Floquet spectrum and overlap of nonlinear resonances in the classical phase space.

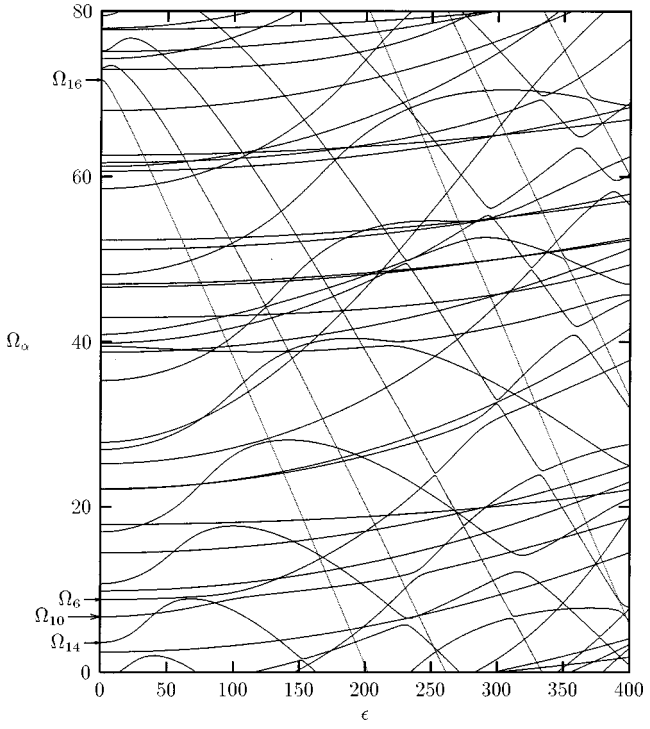

FIG. 9. Plot of quasienergies as a function of field strength for the driven square well. Curves associated with resonance states (i.e., Ω_{16} and Ω_{14}) resemble eigencurves of the Mathieu equation [27]. The avoided crossing discussed in the text is between Ω_6 and Ω_{10} at $\epsilon\approx100$.

Figure 9 shows the quasienergies of the lowest 40 states in our basis. Using a finite basis to calculate quasienergies always introduces numerical error [26], but for the field strengths shown this error is extremely small. At higher field strengths one would need to use a larger basis to avoid numerical error. Essentially one can avoid numerical error as long as the basis extends well into the regular region of the phase space. Since our calculations use states up to $n=80$ we will not experience numerical error until the chaotic region comes near $J=80$, which is not the case for any field strengths we consider here. Note that there are also several places in Fig. 9 where quasienergy curves actually cross each other. These ''apparent crossings'' arise when the quasienergies of two states are in resonance, but transitions between the states are forbidden [25].

One interesting thing to note is that several of the curves (i.e., Ω_{16}, Ω_{14}, ...) in Fig. 9 resemble curves of the characteristic values of Mathieu's equation [27], which is the Schrödinger equation for the quantum pendulum. Husimi plots of states with these quasienergies are localized inside the pendulumlike nonlinear resonance [similar to Fig. 6(b)]. At very high field strengths, where the classical resonance has been destroyed, the quasienergy curves have gone through many avoided crossings and no longer resemble the eigencurves of the Mathieu equation.

Avoided level crossings provide one of the two mechanisms available for population transfer between Floquet states. The other mechanism is a nonadiabatic turn-on of the driving field. If the field is turned on rapidly, transitions between Floquet states will be allowed because the Floquet states at one field strength will not be Floquet states at another field strength. A rapidly varying field strength leads to rapid changes in the structure of the Floquet states and thus to transitions between Floquet states. However, if the field is turned on adiabatically the system will remain in the same (continuously connected) Floquet state until it reaches an avoided crossing. We will confine our investigation to population transfer that occurs at the avoided crossing between Ω_6 and Ω_{10} at $\epsilon\approx100$.

To study this avoided crossing we start with the system in $n=6$ and investigate the behavior of the system for field strengths below and above the avoided crossing. At $\epsilon=65$ the state is composed of 98.6% $|\Omega_6\rangle$ and 1.4% $|\Omega_{10}\rangle$ at the end of its turn-on. At $\epsilon=125$ we are mostly through the avoided crossing and the state is composed of 72.5% $|\Omega_{10}\rangle$

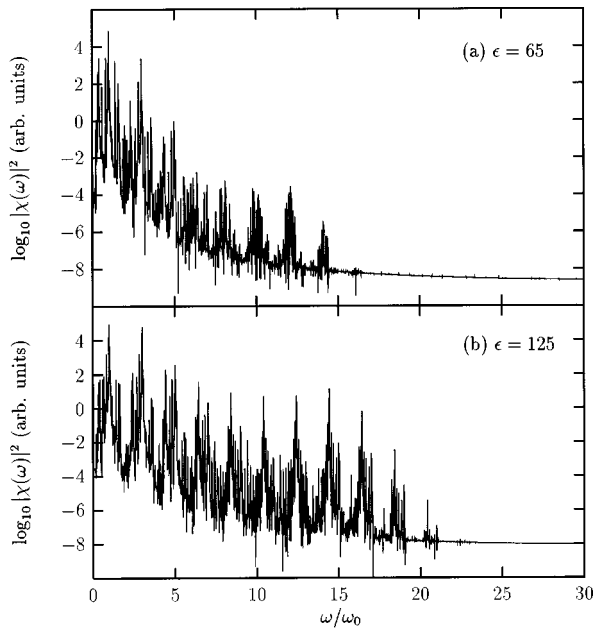

FIG. 10. Spectra for the driven square well with initial condition $n=6$. The avoided crossing between Ω_6 and Ω_{10} occurs between these two field strengths. Note the increase in HHG after the system has passed through the avoided crossing.

and 27.5% $|\Omega_6\rangle$. Spectra shown in Fig. 10 show an increase in HHG as the system traverses the avoided crossing. This indicates that population transfer ''spreads'' the wave function over a wider range of energies.

Since this avoided crossing is so broad we can easily monitor the change in the Husimi distributions of the Floquet states. Figure 11 shows the Husimi distributions for $|\Omega_6\rangle$ and $|\Omega_{10}\rangle$ at various field strengths. At $\epsilon=65$ we see that $|\Omega_{10}\rangle$ sits at higher energy than $|\Omega_6\rangle$. At $\epsilon=100$ both states are in approximately the same region of phase space. At $\epsilon=125$ $|\Omega_6\rangle$ sits at higher energy than $|\Omega_{10}\rangle$. The Husimi distributions of the two Floquet states have ''flowed'' through each other. Since these Floquet states are associated with unstable periodic orbits of the classical system, it is clear that avoided crossings occur when these periodic orbits move past each other in phase space. Since periodic orbits can cross only after the destruction of Kolmogorov-Arnold-Moser tori in classical phase space when nonlinear resonances overlap, we see that there is a close connection between chaos and avoided crossings.

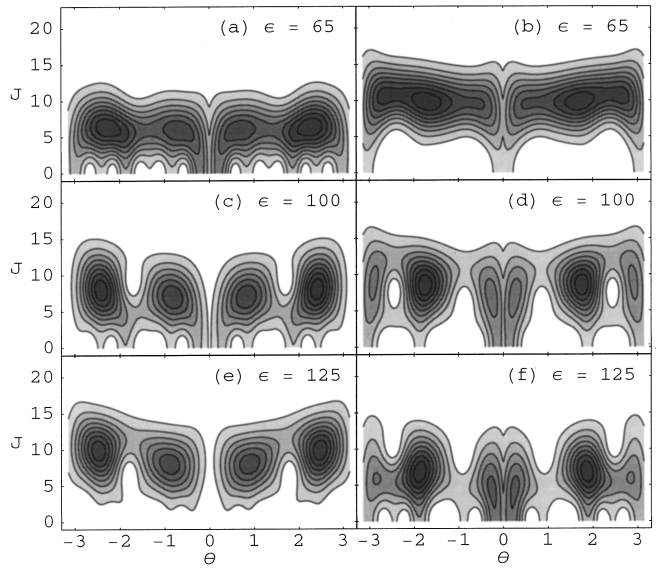

FIG. 11. Husimi plots for (a), (c), and (e) $|\Omega_6\rangle$ and (b), (d), and (f) $|\Omega_{10}\rangle$. Note how the two states flow through each other as they move through the avoided crossing.

Avoided crossings increase HHG in two ways. The first is by creating a superposition of Floquet states that occupy different regions of phase space. This superposition will typically be spread over a wide range of energies, which leads to the plateau structure that is observed in the radiation spectra. The second way avoided crossings contribute to HHG is by creating delocalized Floquet states. After a state passes through many avoided crossings it will lose the close association it had with a single periodic orbit and become associated with a large set of periodic orbits. These periodic orbits will typically be spread throughout the chaotic region, which leads to delocalization of the Floquet state.

VI. CONCLUSIONS AND DISCUSSION

We have studied the radiation spectrum of two strongly driven multilevel systems whose classical counterparts exhibit bounded chaos. The quantum systems show the highest harmonic generation when the corresponding classical systems become chaotic. This can be due to broadening of individual Floquet states across classically chaotic regions or the population of multiple Floquet states with support on chaotic regions. We observe the characteristic HHG plateau structure in either case. The harmonic cutoff is determined by the energy range spanned by the populated Floquet states. In analogy with the harmonic cutoffs of the two-level model and tunnel ionization process, the cutoff is determined by the kinetic energy attainable from the driving field. We expect this relation to be applicable to all multilevel models exhibiting bounded chaos. Our results may also be applicable in atomic systems where bound-bound transitions account for most or all of the radiation. However, it should be pointed out that in typical atomic systems chaos is not bounded and leads to ionization.

Chaos is also connected to the onset of the avoided level crossings in the quasienergy spectrum. One method that can be used to excite Floquet states other than those adiabatically connected to the initial state is to run the system through an avoided crossing. Population transfer at avoided crossings can lead to quite significant changes in the Floquet composition of the wave function. This possibility seems to hold the most promise for engineering a superposition of Floquet states that will radiate high-order harmonics of the driving field.

ACKNOWLEDGMENTS

The authors wish to thank the Welch Foundation (Grant No. F-1051) and DOE (Contract No. DE-FG03-94ER14465) for partial support of this work. We also thank the University of Texas at Austin High Performance Computing Center for use of their computer facilities.

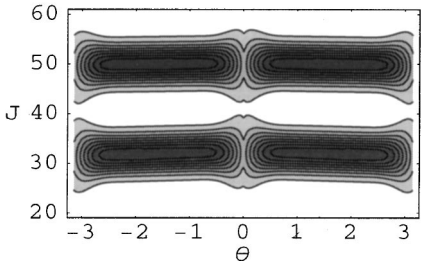

FIG. 12. Husimi plot showing the two states in the superposition. $|\Omega_{32}\rangle$ is primarily composed of the $n=32$ energy eigenstate, while $|\Omega_{50}\rangle$ is composed mainly of $n=50$.

APPENDIX A: THE HUSIMI DISTRIBUTION

The Husimi distribution is a quasiprobability distribution function allowing direct comparison with classical phase space distribution functions [28,29]. The quantum-mechanical phase space is constructed by adopting the coherent state basis. A coherent state is a minimum uncertainty wave packet centered at a point (x_0,p_0) in the phase space. In the position and momentum representation they are given as [30,31]

$$\langle x|x_0,p_0\rangle=\left(\frac{1}{\sigma^2\pi}\right)^{1/4}\times\exp\left(-\frac{(x-x_0)^2}{2\sigma^2}+\frac{ip_0(x-x_0)}{\hbar}\right) \quad \text{(A1)}$$

and

$$\langle p|x_0,p_0\rangle=\left(\frac{\sigma^2}{\pi\hbar^2}\right)^{1/4}\times\exp\left(-\frac{\sigma^2(p-p_0)^2}{2\hbar^2}-\frac{ix_0(p-p_0)}{\hbar}\right), \quad \text{(A2)}$$

where σ is a squeezing parameter that determines the width of the Gaussian wave packet in each dimension. The Husimi distribution function $W(x_0,p_0)$ for an arbitrary wave function is just $|\langle\psi|x_0,p_0\rangle|^2$, which is the probability that a particle lies within an area $\hbar$ centered at (x_0,p_0).

APPENDIX B: RADIATION SPECTRUM FOR A SUPERPOSITION OF FLOQUET STATES

In this appendix we will examine the radiation spectrum of a superposition of two Floquet states that have support on disjoint sets of unperturbed energy eigenstates. Husimi plots of these states are shown in Fig. 12. We will write the superposition as

$$|\psi(t)\rangle=a_\alpha e^{-i\Omega_\alpha t}|\Omega_\alpha(t)\rangle+a_\beta e^{-i\Omega_\alpha t}|\Omega_\beta(t)\rangle, \quad \text{(B1)}$$

where $|a_\alpha|^2+|a_\beta|^2=1$ and $|\Omega(t)\rangle=|\Omega(t+T)\rangle$.

The time-dependent dipole expectation value for this superposition is

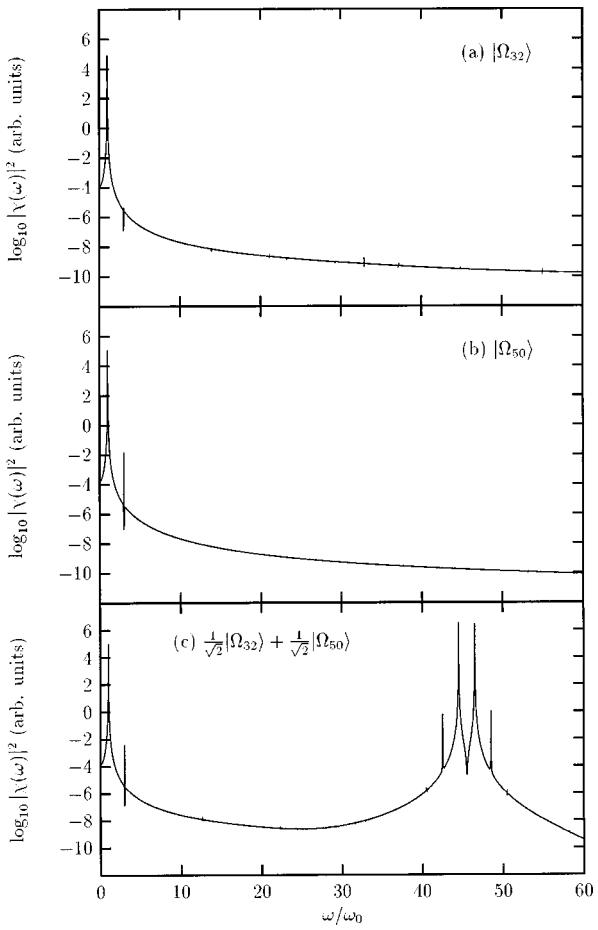

FIG. 13. Spectra for (a) and (b) individual Floquet states and (c) a superposition of two states. The location of the cluster of peaks in (c) is determined by the separation in energy of the Husimi distributions in Fig. 12.

$$\langle\psi(t)|x|\psi(t)\rangle=|a_\alpha|^2\langle\Omega_\alpha(t)|x|\Omega_\alpha(t)\rangle+|a_\beta|^2\langle\Omega_\beta(t)|x|\Omega_\beta(t)\rangle+a_\alpha^* a_\beta e^{i(\Omega_\alpha-\Omega_\beta)t}\langle\Omega_\alpha(t)|x|\Omega_\beta(t)\rangle+a_\beta^* a_\alpha e^{i(\Omega_\beta-\Omega_\alpha)t}\langle\Omega_\beta(t)|x|\Omega_\alpha(t)\rangle. \quad \text{(B2)}$$

The first two terms correspond to the dipole value if the system was in a single Floquet state $|\Omega_\alpha(t)\rangle$ or $|\Omega_\beta(t)\rangle$. A single Floquet state radiates only at the harmonics of the driving field. Since these terms correspond to transitions within a single Floquet state, the harmonic production will be determined by the range of unperturbed energy eigenstates over which that Floquet state has support. If the Floquet state is spread over a wide range of energies, then these terms can contribute HHG. If the Floquet state is confined to a narrow band of energies there will be no HHG. Figure 12 shows two Floquet states that lie in the regular region of the phase space for the driven square well at $\epsilon=50$. Radiation spectra for each of these states are shown in Figs. 13(a) and

13(b). It is clear that these states do not generate high harmonics, as predicted.

The last two terms in Eq. (B2) are cross terms that correspond to transitions between the two Floquet states. Transitions between Floquet states give rise to radiation at frequencies $n\omega_0 \pm (\Omega_\alpha - \Omega_\beta)$. If the two Floquet states have support on widely separated sets of energy eigenstates, then these terms can lead to HHG (at shifted harmonics). An example of this is shown in Fig. 13(c), which shows the radiation spectrum for a superposition of the two states shown in Fig. 12. Note that one of these Floquet states has most of its support on the $n=32$ energy eigenstate and the other Floquet state is concentrated near $n=50$. We expect the superposition to radiate at frequencies corresponding to the difference in these energies. For $\omega_0=80$ this is near the 45th harmonic, which is exactly where the cluster of peaks in Fig. 13(c) appears. The width of this cluster is determined by the range of energies over which the two Floquet states have support. Close inspection of the peaks in Fig. 13(c) shows that they are all shifted by 0.477 from the odd harmonics. This agrees with our expectations since the difference in the quasienergies of the two Floquet states (divided by ω_0) is $(\Omega_{32} - \Omega_{50})/80 = (46.712 - 8.526)/80 = 0.477$.

[1] L. V. Keldysh, Sov. Phys. JETP **20**, 1307 (1965).
[2] M. Lewenstein, Ph. Balcou, M. Yu. Ivanov, Anne L'Huillier, and P. B. Corkum, Phys. Rev. A **49**, 2117 (1994).
[3] P. B. Corkum, Phys. Rev. Lett. **71**, 1994 (1993).
[4] K. C. Kulander, K. J. Schafer, and J. L. Krause, in *Proceedings of the Super-Intense Laser-Atom Physics III Workshop*, Vol. 316 of *NATO Advanced Study Institute, Series B: Physics*, edited by B. Piraux *et al.* (Plenum, New York, 1993).
[5] Bala Sundaram and Peter W. Milonni, Phys. Rev. A **41**, 6571 (1990).
[6] S. Cocke and L. E. Reichl, Phys. Rev. A **53**, 1746 (1996).
[7] Ph. Balcou, Anne L'Huiller, and D. Escande, Phys. Rev. A **53**, 3456 (1996).
[8] F. I. Gauthey, C. H. Keitel, P. L. Knight, and A. Maquet, Phys. Rev. A **55**, 615 (1997).
[9] L. E. Reichl, *The Transition to Chaos In Conservative Classical Systems: Quantum Manifestations* (Springer-Verlag, Berlin, 1983).
[10] Vitali Averbukh and Nimrod Moiseyev, Phys. Rev. A **51**, 3911 (1995).
[11] J. H. Shirley, Phys. Rev. **138**, B979 (1965).
[12] H. Sambe, Phys. Rev. A **7**, 2203 (1973).
[13] D. F. Escande and F. Doveil, J. Stat. Phys. **26**, 257 (1981).
[14] G. Gabrielse and H. Dehmelt, Phys. Rev. Lett. **55**, 67 (1985).
[15] A. R. Kolovsky, in *Chaos—The Interplay Between Stochastic and Deterministic Behavior*, edited by P. Garbaczewski *et al.* (Springer-Verlag, Berlin, 1995).
[16] G. O. Morrow and L. E. Reichl, Phys. Rev. A **50**, 2027 (1994).
[17] W. A. Lin and L. E. Reichl, Phys. Rev. A **40**, 1055 (1989).
[18] L. E. Reichl, Phys. Rev. A **39**, 4817 (1989).
[19] M. L. Pons, R. Taïeb, and A. Maquet, Phys. Rev. A **54**, 3634 (1996).
[20] J. Kamiński, Phys. Lett. A **151**, 308 (1990).
[21] W. A. Lin and L. E. Reichl, Physica D **19**, 145 (1986).
[22] M. Z. Fuka, J. K. McIver, W. Becker, M. Orszag, and R. Ramí rez, Phys. Rev. E **51**, 1935 (1995).
[23] W. A. Lin and L. E. Reichl, Phys. Rev. A **37**, 3972 (1988).
[24] J. Y. Shin and H. W. Lee, Phys. Rev. E **50**, 902 (1994).
[25] H. P. Breuer, K. Dietz, and M. Holthaus, Z. Phys. D **8**, 349 (1988).
[26] H. P. Breuer and M. Holthaus, Z. Phys. D **11**, 1 (1989).
[27] See *Handbook of Mathematical Functions*, Natl. Bur. Stand. Appl. Math. Ser. No. 55, edited by M. Abramowitz and I. A. Stegun (U.S. GPO, Washington, DC, 1968).
[28] K. Husimi, Proc. Phys. Math. Soc. Jpn. **22**, 246 (1940).
[29] K. Takahashi, Prog. Theor. Phys. Suppl. **98**, 109 (1989).
[30] S. J. Chang and K. J. Shi, Phys. Rev. A **34**, 7 (1986).
[31] B. Crespi, G. Perez, and S. J. Chang, Phys. Rev. E **47**, 986 (1993).